TIME-VARYING INVERSE FILTERING FOR HIGH RESOLUTION IMAGING WITH ULTRASONIC GUIDED WAVES

Jochen Moll, Claus-Peter Fritzen
University of Siegen, Institute of Mechanics and Automatic Control – Mechatronics,
Paul-Bonatz-Straße 9-11, 57076 Siegen, Germany, E-Mail: moll@imr.mb.uni-siegen.de

ABSTRACT

Active strategies for structural health monitoring using ultrasonic guided waves mainly deal with excitation signals that are band-limited in order to minimize the effect of dispersion. The underlying idea is to activate only the fundamental wave-modes so that the signal complexity decreases. However, it would be advantageous to increase the temporal resolution of the signal in order to enhance the performance of the post-processing algorithms.

This paper suggests a new technique that deconvolves narrowband and non-stationary ultrasonic signals by means of a time-varying inverse Filter. The filter is realized through the application of the matching pursuit decomposition algorithm. As a result one attains ultrasonic signals where the waveforms have a significantly smaller temporal extent compared to the original signals, resulting in a much higher resolution. After automatically deconvolving the ultrasonic signals they are applied on the time-difference-of-arrival (TDOA) and time-of-arrival (TOA) imaging algorithms. It can be observed from the images that the point spread function becomes significantly smaller. Thus, it can be possible in the future to image not only the correct position of the damage but also the size and in case of a crack the corresponding orientation.

INTRODUCTION

Permanently mounted sensors arranged as a spatially distributed sensor network are being considered for monitoring the integrity of structural components like a fuselage section of an aircraft or a rotor blade of a wind energy plant. In contrast to non-destructive testing (NDT) approaches, where the sensors are normally not permanently fixed, baseline measurements become available. Subsequent deviations from these reference measurements can be either referred to structural degradation, changing environmental and operational conditions (e.g. temperature, vibrations) or sensor faults. In this study it is assumed that the changing conditions can be controlled either by temperature compensation [1, 2] or filtering strategies [3] and that the piezoelectric sensors are intact.

The strategy in this paper is to use ultrasonic guided waves that are emitted from piezoelectric actuators. Once initiated, they travel across the structure and interact with different types of defects like holes, delaminations etc. An important characteristic of these waves is dispersion, which means that the wave velocity is a function of frequency and thickness of the material. Because of that it is not possible to use a broad-band impulse excitation signal that gets heavily distorted while propagating across the structure. However, this kind of excitation signal would be desirable, because it has minimum temporal extent and thus maximum resolution. Instead of an impulse, it is a common strategy to use band-limited excitation signals in the lower *fd*-range to activate only the fundamental wave modes.

In this paper a narrow-band excitation is used to simulate wave propagation with the spectral element method in an isotropic plate [4]. The resulting sensor signals are recorded by a sparse number of piezoelectric sensors aligned in a spatially distributed sensor network. In order to receive as much information about the defect as possible the common source technique is used to record signals from all possible actuator-sensor combinations. The signals are automatically processed with the time-varying inverse filter to transform them to broad-band and highly resolved signals (see reference [5]). Subsequently, these signals are used in the time-of-arrival and time-difference-of-arrival algorithms in order to determine the damage position tomographically.

SIGNAL PROCESSING TECHNIQUES

TIME-INVARIANT WIENER FILTER

Figure 1 schematically shows the convolution process to get the non-stationary sensor signal *s(t)*. First, an initial toneburst signal $s_0(t)$ starting at $t=0$ is convolved with a reflectivity function *g(t)*. The reflectivity function symbolically shows structural reflectors like boundaries or stringers. Then noise *n(t)* is added to the convolved signal to get the final echo signal *s(t)*.

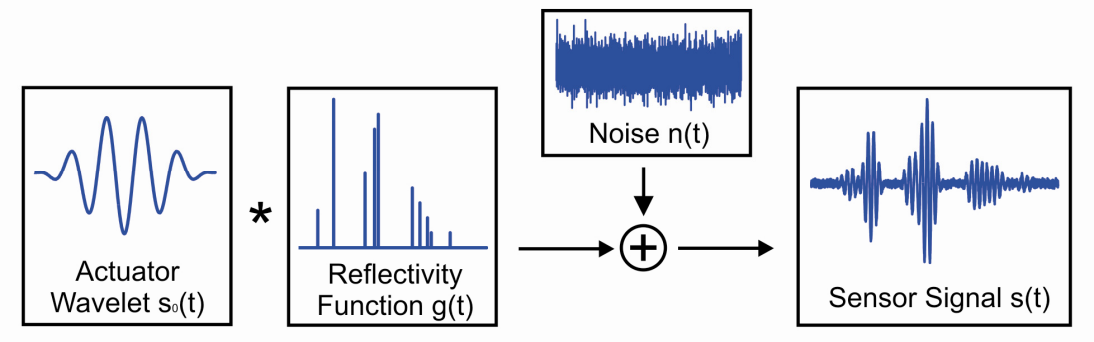

Figure 1: Schematic visualization of the convolution process

Mathematically, the convolution can be expressed in time domain as

$$s_0(t) * g(t) + n(t) = s(t). \tag{1}$$

Transforming this relationship into the Fourier domain results in an equivalent expression where the convolution operation (*) is replaced by a multiplication:

$$S_0(f)G(f) + N(f) = S(f) \tag{2}$$

Equation (2) can be rearranged to get the final Wiener filter solution *W(f)*

$$G(f) = W(f)S(f) = \frac{S_0^*(f)}{|S_0(f)|^2 + \frac{P_N(f)}{P_G(f)}} S(f). \tag{3}$$

In this equation $S_0^*(f)$ denotes the complex conjugate of $S_0(f)$ and *W(f)* the Wiener filter. $P_N(f)$ and $P_G(f)$ are the power spectral densities of noise and reflectivity function, respectively. The latter can be iteratively estimated for the optimal Wiener filter as proposed in [6]. The solution for the Wiener Filter simplifies to the inverse filter when $P_N(f)$ tends to zero. In this case *G(f)* can be calculated via

$$G(f) = \frac{1}{S_0(f)} S(f). \tag{4}$$

The inverse Fourier transform yields the desired time domain reflectivity function *g(t)*.

MATCHING PURSUIT DECOMPOSITION ALGORITHM

The Matching Pursuit (MP-) algorithm has been originally introduced by MALLAT AND ZHANG [7] and successfully applied in structural health monitoring by different researchers [8-11]. It decomposes a signal into a linear combination of analytical functions (so-called atoms) that are selected from a redundant database of atoms which is termed dictionary. The atom from the dictionary that matches the signal best is selected for reconstruction. The algorithm terminates automatically when the signal energy of the residuum after *n* iterations $r_{n+1}(t)$ falls below a pre-defined threshold of e.g. 5% of the original signal energy or when the maximum number of iterations are exceeded. Mathematically, this

iterative procedure can be written in the following five steps, where the residuum $r_0(t)$ equals the sensor signal $s(t)$ in the first iteration:

Step 1: Create a dictionary D using Gabor atoms y_G (see equation (8)).

Step 2: Select the best match between each atom of the dictionary $y_m(t)$ and the residuum $r_n(t)$ in iteration n by means of the highest absolute correlation.

$$y_{m,n} = \arg\max_{y_m \in D} \left| \left\langle r_n(t), y_m(t) \right\rangle \right| \tag{5}$$

Step 3: Subtract the atom $y_{m,n}$ which is the best match in iteration n with the residuum $r_n(t)$.

$$r_{n+1} = r_n(t) - \left\langle r_n(t), y_{m,n}(t) \right\rangle y_{m,n} \tag{6}$$

Step 4: Add this signal to the reconstruction $s'(t)$.

$$s'(t)_{n+1} = s'_n(t) + \left\langle r_n(t), y_{m,n}(t) \right\rangle y_{m,n} \tag{7}$$

Step 5: Repeat steps 2 → 5 until either the pre-defined threshold or the maximum number of iterations is reached.

Here, the m-th Gabor atom with the four parameters $[s_m, u_m, \omega_m, \varphi_m]$ is defined similar to [8] as

$$y_{G,m}(t) = \mathrm{Re}\left\{ \frac{1}{\sqrt{s_m}} 2^{\frac{1}{4}} e^{-\pi\left(\frac{t-u_m}{s_m}\right)^2} e^{i\omega_m t} e^{i\varphi_m} \right\} \tag{8}$$

where s_m represents a scaling parameter, u_m the time center, ω_m the angular frequency and φ_m the phase.

The design of the dictionary is a compromise between computational efficiency and reconstruction accuracy. Compared to other implementations the size of the dictionary is relatively sparse and special attention is put on the reconstruction of the primary waveform because this part of the waveform represents the first interaction with damage. In case of active excitation, the dictionary can be chosen with the knowledge about the excitation signal. Thus, the angular frequency matches the center frequency of the actuator wavelet. The parameter interval of s and u is discretized using a reasonable choice with respect to the shape of the actuator pulse. In contrast to the parameters s and u, which are adapted by the highest absolute correlation, φ is optimized a posteriori during the iterations. A statistical post-processing technique has been applied to reject all these MP-reconstructions that have amplitudes smaller than one percent of adjacent peaks. The distance of adjacent peaks is defined by plus-minus half of the duration of the actuator wavelet. This step is important to avoid over-fitting.

The matching pursuit decomposition algorithm reconstructs an ultrasonic signal adaptively and rejects additive noise. Thus, it has inherent filtering properties. Moreover, each atom consists of only a few parameters. By storing these parameters instead of all sample points memory can be saved which is particularly important for energy harvesting in wireless communication systems [12, 13].

TIME-VARYING INVERSE FILTER

This section introduces the design of a time-variant inverse filter that uses the matching pursuit algorithm to provide noise-free representations of the original ultrasonic signal. The noise-free assumption allows to use equation (4) for the inverse Filter instead of the Wiener solution of equation (3). Based on the previous section the reflectivity function can be calculated as the sum of N individual reflectivity functions $G_k(f)$. Here, N is the number of iterations in the matching pursuit before it terminates.

$$g(t) = \sum_{k=1}^{N} \left| IFFT\left\{ G_k(f) \right\} \right| = \sum_{k=1}^{N} \left| IFFT\left\{ \frac{1}{S_{0,k}(f)} S_k(f) \right\} \right| \tag{9}$$

In this equation $S_{0,k}(f)$ and $S_k(f)$ represent the Fourier transforms of the k-th atom with the difference that the time origin of $S_{0,k}(f)$ is at $t=0$. It can be concluded that both spectra have the same amplitude but a different phase spectrum. However, the spectral division locates the spike according to the temporal position of the atom. The absolute value of $g(t)$ has been chosen without loss of generality (compare the absolute value of the Hilbert envelope). With the aid of this operation negative interferences during the imaging procedure can be avoided.

LOCALIZATION ALGORITHMS

The time-of-arrival (TOA) and the time-difference-of-arrival (TDOA) algorithms have been used in the literature for damage visualization. In this paper only the time-of-arrival approach will be introduced mathematically. The reader is forwarded to [14] for a theoretical introduction of the TDOA algorithm. Both techniques are based on differential signals between pristine and damaged structure. The advantage of using differential signals compared to other localization strategies is the fact that reflections from structural boundaries and direct arrivals are eliminated. Thus, the differential signal contains information about the wave-damage interaction only. Challenging tasks are the synchronization of the measurement equipment and the compensation of the temperature effect [1].

Figure 2 shows the geometric relationships of the time-of-arrival algorithm. The intensity value $I_P(x,y)$ at the image position $P(x,y)$ is extracted from the differential signal. This value corresponds to a travel time t_{ij} of the wave from the actuator i across the position $P(x,y)$ to the sensor position j. Based on a constant group velocity c_{Gr} the travel time t_{ij} can be determined by:

$$t_{ij}(x,y) = \frac{1}{c_{Gr}}\left(d_{iP} + d_{Pj}\right) = \frac{1}{c_{Gr}}\left(\sqrt{x_i^2 + y_i^2} + \sqrt{x_j^2 + y_j^2}\right) \tag{10}$$

Based on t_{ij} the intensity $I_P(x,y)$ can be calculated for all actuator-sensor combinations via

$$I_P(x,y) = \sum_{i=1}^{M-1} \sum_{j=i+1}^{M} e_{ij}\left(t_{ij}(x,y)\right). \tag{11}$$

In this equation e_{ij} denotes the differential signal between the actuator-sensor pair i-j. The double sum in equation (11) contains the information of the common-source technique while the number of sensor is represented by M. In practical applications not the radio-frequency but the envelope-detected signals are used in order to avoid local interferences [15]. In this paper the differential signal e_{ij} is processed with the Hilbert envelope as well as the proposed time-varying inverse filter.

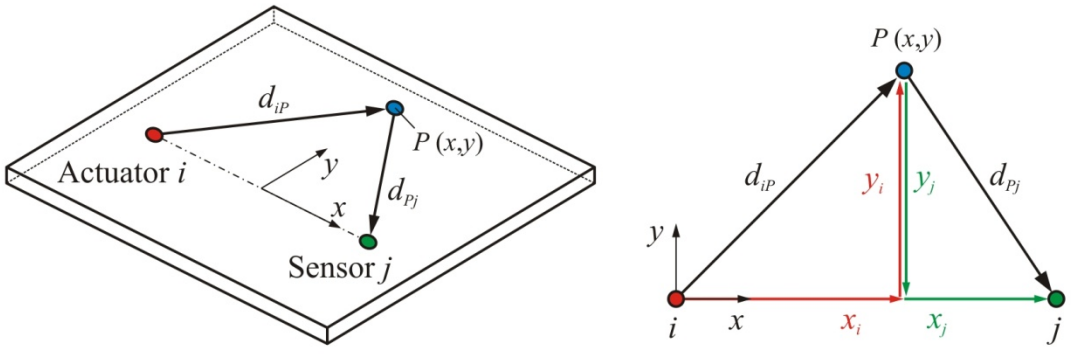

Figure 2: Geometric relationships of the time-of-arrival algorithm

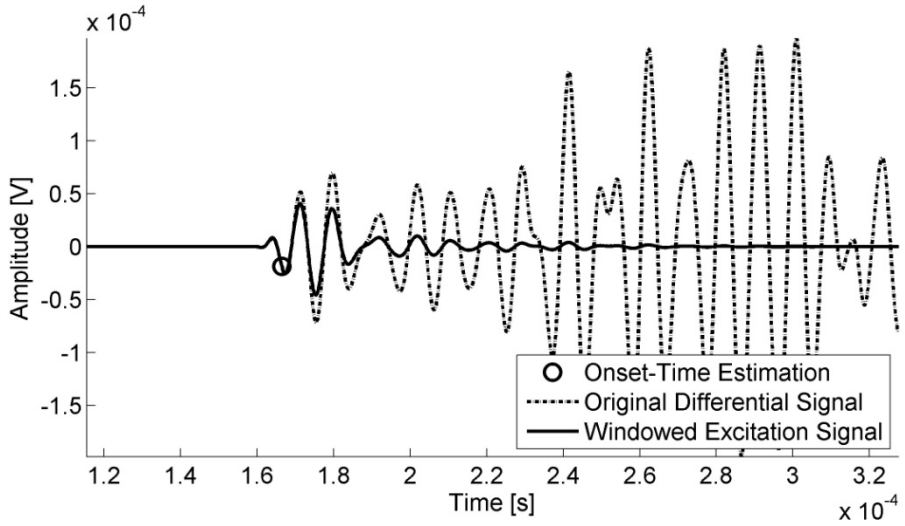

Figure 3: Illustration of the exponential windowing; the influence of secondary reflections decrease through the weighting

In [15] an exponential window *w(t)* has been introduced in order to weight secondary reflections of the signal. Mathematically, this windowing function is defined as

$$w(t) = e^{-\frac{(t-t_0)}{\varepsilon}} \tag{12}$$

In this formula t_0 represents the onset-time of the differential signal that can be detected automatically by means of an energy-based algorithm [16]. As a result, the weighting function is one at t_0 and decays exponentially with the decay rate ε. Figure 3 illustrates the weighting with a radio-frequency signal. The original differential signal contains many secondary reflections. Applying the onset-time estimation algorithm the beginning of the signal can be extracted automatically. Multiplying the windowing function using a decay rate of $\varepsilon=2\cdot10^{-5}$ with the original differential signal the influence of secondary reflections decrease.

EXPERIMENTAL SETUP

The spectral element method has been used in this study to simulate wave propagation in an aluminum plate. Isotropic material properties have been chosen because the tomography algorithms are

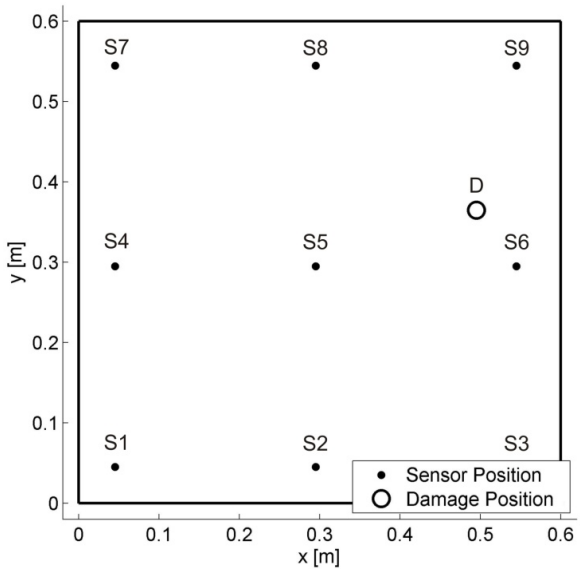

Figure 4: Experimental setup

Table 1. Coordinates of the sensor positions

	x-coordinate [m]	*y-coordinate [m]*
S_1	*0.045*	*0.045*
S_2	*0.295*	*0.045*
S_3	*0.545*	*0.045*
S_4	*0.045*	*0.295*
S_5	*0.295*	*0.295*
S_6	*0.545*	*0.295*
S_7	*0.045*	*0.545*
S_8	*0.295*	*0.545*
S_9	*0.545*	*0.545*

Table 2. Coordinates of the damage position

	x-coordinate [m]	*y-coordinate [m]*
D	*0.495*	*0.365*

not able so far to deal with anisotropy like other damage localization formulations [17, 18]. The dimension of the plate is 600mm x 600mm x 1.5mm (see Figure 4). Nine piezoelectric sensors are arranged across the plate and the sensor coordinates are listed in Table 1. A 3-cycle Hann-windowed toneburst with 100kHz center frequency is used for excitation. The S_0-mode has been chosen in this study exclusively, because the wave-velocity is higher compared to the A_0-mode. Consequently, the first waveform in the differential signal comes from the S_0-mode that has a wave velocity at this frequency-thickness product of 5409m/s. Damage has been modeled by reducing the stiffness of a single 10mm by 10mm element of twenty percent. The damage coordinates are listed in Table 2.

RESULTS

Figure 5 shows two exemplary actuator-sensor combinations, the appropriate MP-reconstruction and the corresponding deconvolution. It can be seen from this figure that the onset-time of each time-trace can be reconstructed precisely. Moreover, the temporal resolution can be improved significantly. The properties of the matching pursuit algorithm allow to approximate the number of physical waveforms in the sensor signal, because the sensor signal represents a superposition of time-delayed and phase-shifted actuator wavelets. Unfortunately, it is not possible to guarantee that the correct number of waveforms is reconstructed.

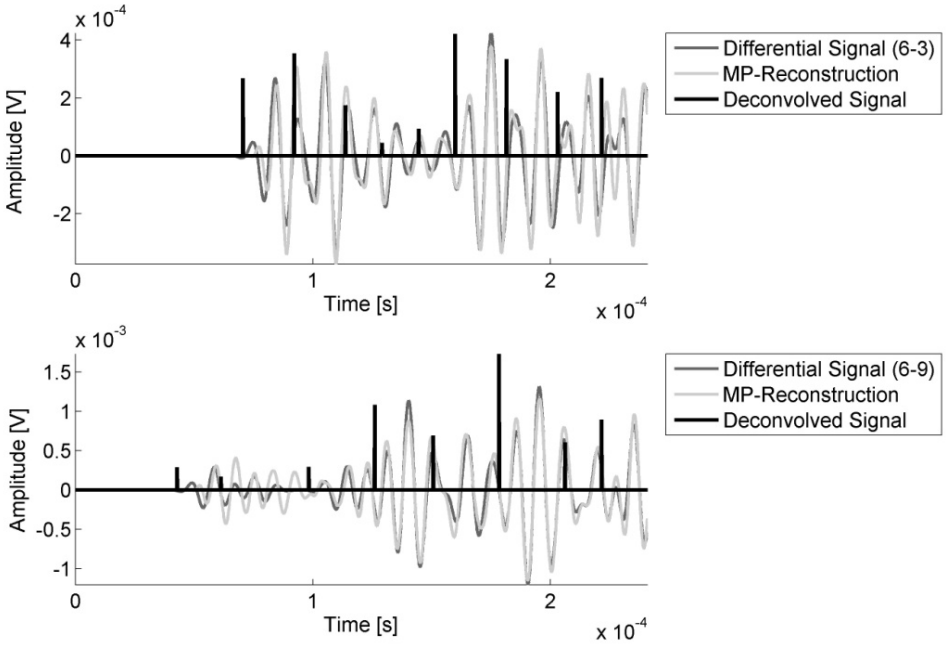

Figure 5: Improved temporal resolution of the differential signal by means of time-varying inverse filtering for actuator-sensor pair 6-3 (top) and 6-9 (bottom)

Applying the processed signals directly to the visualization routines seems to be impractical for two reasons: The first reason refers to the procedure how the damage map is constructed. Therefore, the plate is discretized equidistantly in *x*- and *y*-direction with a certain spatial resolution. In order to assign a value to a pixel position the resolution must be incredibly high to avoid spatial aliasing. The second problem refers to inaccuracies in reconstructing the onset-times of the time-traces and uncertainties in the underlying wave velocities. In order to solve both problems and to design the method more robust a Gaussian window with the standard deviation σ is centered on the peak positions while keeping the original amplitudes (see Figure 6). Thus, each peak gets a certain temporal dimension, where the highest damage probability remains at the peak position.

Figure 7 shows damage maps for the time-of-arrival and time-difference-of-arrival algorithms for a single actuator-sensor pair and a single actuator-sensor-sensor pair, respectively. It can be concluded that the ellipse curve of the TOA algorithm crosses the actual damage position for both, the envelope-detected and the deconvolved signals. The same behavior can be observed in the TDOA-images.

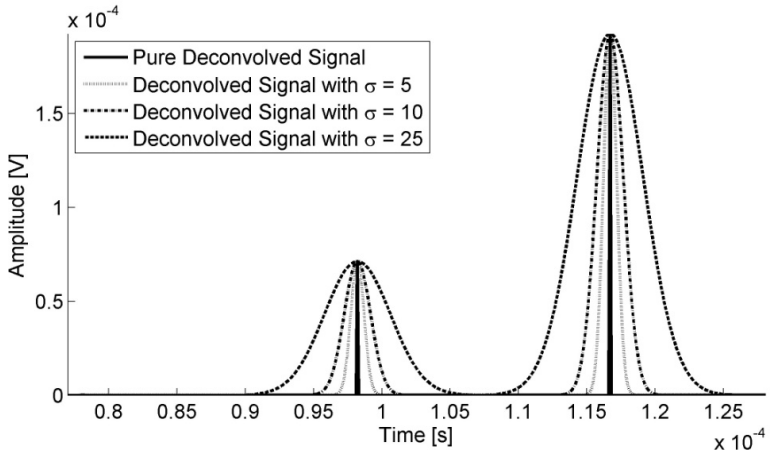

Figure 6: Deconvolved signal with Gaussian window centered on the peak position

Consequently, it is plausible that the image quality by fusing all possible actuator-sensor combinations is higher for the deconvolved signals. As a result of the high-resolution TOA-image of Figure 7 a relationship to the ellipse method can be derived [19]: In contrast to the proposed visualization strategy, where pixel-intensities from a spatial grid are calculated, the ellipse method determines a single curve for each actuator-sensor pair. The damage position is expected to be at those points where different ellipses intersect with the highest density [20]. In ultrasonic tomography the information about the damage location is already included by summing all individual images. Thus, a statistical post-processing is not necessary.

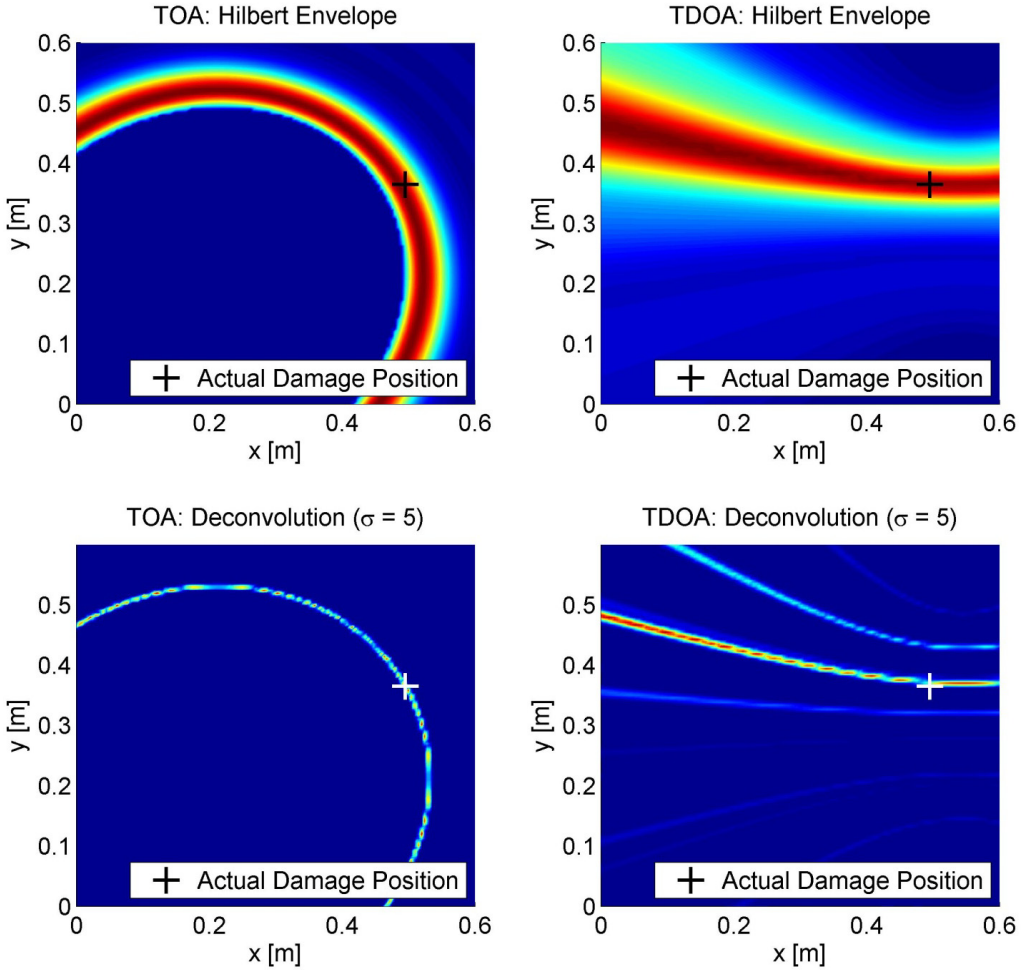

Figure 7: Damage maps constructed by the TOA-Algorithm for a single actuator-sensor pair: Envelope-detected signal (top left) and deconvolved signal (bottom left); Damage maps using the TDOA-Algorithm for a single actuator-sensor-sensor combination: Envelope-detected signal (top right) and deconvolved signal (bottom right)

In a next step, all actuator-sensor combinations have been evaluated for *σ=25*, *σ=10* and *σ=5*. It can be observed from Figure 8 that the TOA algorithm is able to determine the actual damage position with the envelope-detected signals. By choosing the deconvolved signals with the Gaussian modifications the point spread function becomes much smaller compared to the reference case. Unfortunately, the position of the damage is slightly shifted. However, the goal of visualizing a point-like scatterer has been achieved by de-blurring the reference damage map that has been constructed by the envelope-detected differential signals. Thus, for future studies, it seems to be possible to image not only the correct position of the damage but also the size and in case of a crack the corresponding orientation.

The improvement of resolution (especially for σ=5 and σ=10) can be seen via horizontal and vertical cross-sections through the point spread function of the fused images (see Figure 9). The slope of the images with the deconvolved signals is much higher compared to the reference image. Similar results are generated by the TDOA algorithm. Due to lack of space these are not shown here in this paper.

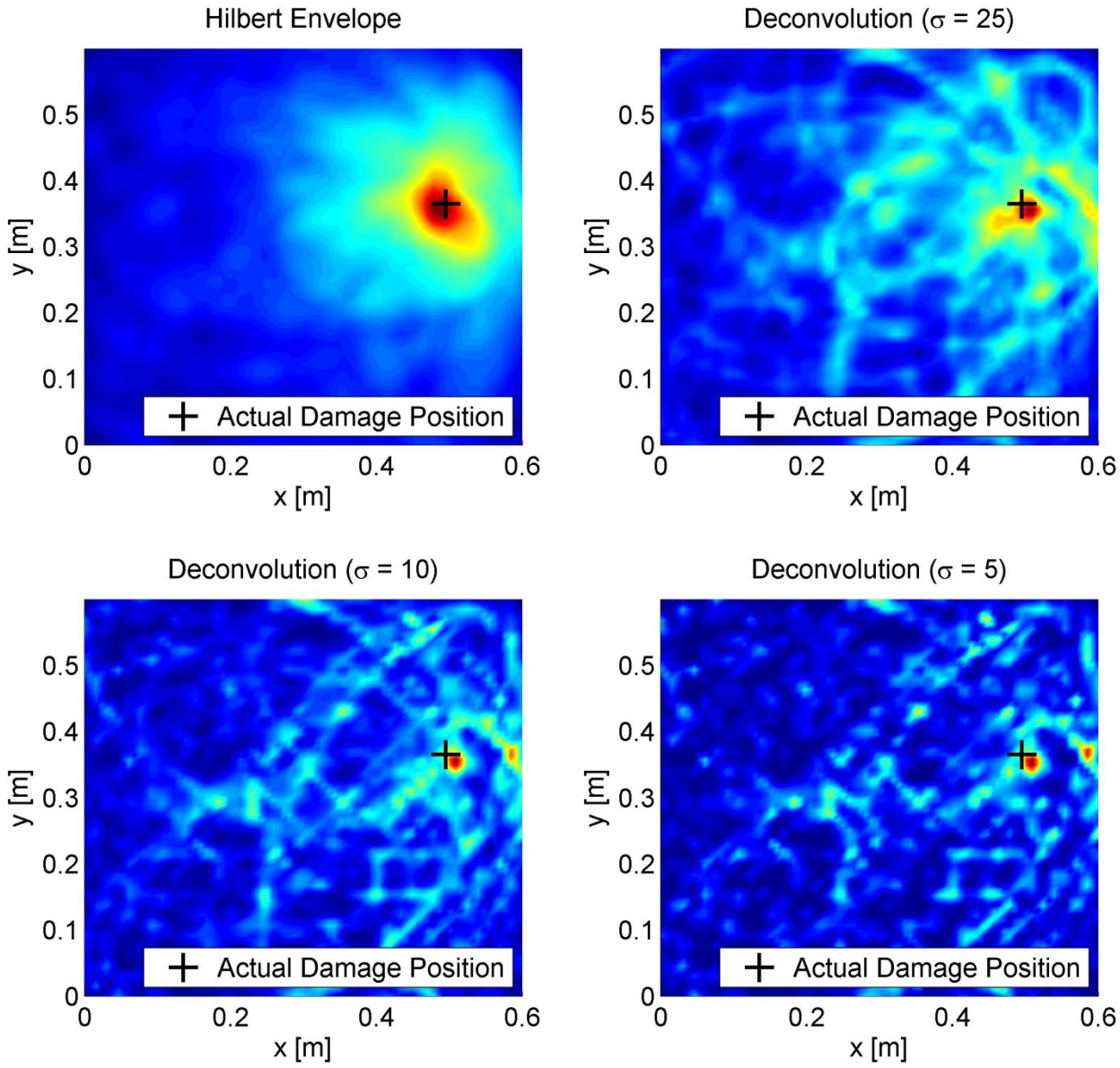

Figure 8: TOA images for all actuator-sensor combinations – Envelope-detected signals (top left), deconvolved signals with σ=25 (top right), σ=10 (bottom left), σ=5 (bottom right)

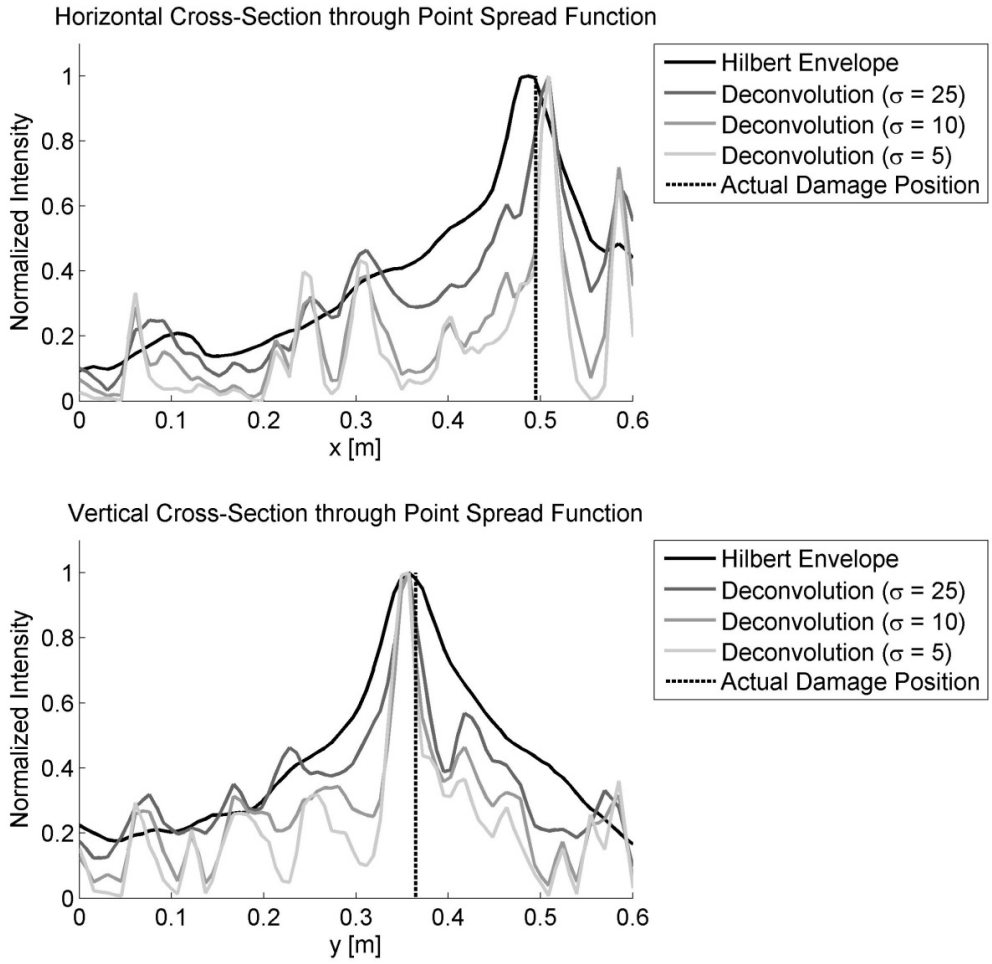

Figure 9: Horizontal and vertical cross-sections through the damage maps of Figure 8

CONCLUSION

The results shown here indicate that the quality of damage localization can be enhanced through the application of a time-varying inverse filter. As a result of the deconvolution procedure the temporal extent of the sensor signal decreases which results in much higher temporal resolution compared to standard envelope-detected signals. Applying the processed signals to the time-of-arrival and time-difference-of-arrival algorithms improves the shape of the point-spread function and deblures the damage map. Furthermore, an automated procedure has been implemented to weight secondary reflections through an exponential window.

In the future, the proposed methodology will be applied to experimental data from an isotropic plate in order to image the orientation of a crack and to size the defect. Furthermore, it is possible to use this signal-processing technique for damage localization in anisotropic structures.

REFERENCES

[1] Croxford A J, Moll J, Wilcox P D and Michaels J E 2009 Efficient Temperature Compensation Strategies for Guided Wave Structural Health Monitoring Ultrasonics

[2] Croxford A J, Wilcox P D, Konstantinidis G and Drinkwater B W 2007 Strategies for guided-wave structural health monitoring Proceedings of the Royal Society A 463 2961-2981

[3] Qing X P, Beard S J, Kumar A, Sullivan K, Aguilar R, Merchant M and Taniguchi M 2008 The performance of a piezoelectric-sensor-based SHM system under a combined cryogenic temperature and vibration environment Smart Materials and Structures 17 1-11
[4] Schulte R T and Fritzen C-P 2008 Spectral Element Modelling of Wave Propagation in Stringer Stiffened Structures *4th European Workshop on Structural Health Monitoring (Krakow, Poland)* 512-519
[5] Moll J and Fritzen C-P 2010 Time-Varying Inverse Filtering of Narrowband Ultrasonic Signals Structural Health Monitoring (submitted for publication)
[6] Cicero T, Cawley P, Simonetti F and Rokhlin S I 2009 Potential and Limitations of a deconvolution Approach for Guided Wave Structural Health Monitoring Structural Health Monitoring 7 51 1-16
[7] Mallat S G and Zhang Z 1993 Matching Pursuits With Time-Frequency Dictionaries IEEE Transactions on Signal Processing 41 12 3397-3415
[8] Raghavan A and Cesnik C E S 2007 Guided-wave signal processing using chirplet matching pursuits and mode correlation for structural health monitoring Smart Materials and Structures 16 355-366
[9] Lu Y and Michaels J E 2008 Numerical Implementation of Matching Pursuit for the Analysis of Complex Ultrasonic Signals IEEE Transactions on Ultrasonics, Ferroelectrics and Frequency Control 55 1 173-182
[10] Zhou W, Chakrabotry D, Kovvali N, Papandreou-Suppappola A, Cochran D and Chattopadhyay A 2007 Damage Classification for Structural Health Monitoring Using Time-Frequency Feature Extraction and Continuous Hidden Markov Models *IEEE Asilomar Conference on Signals, Systems and Computers* 848-852
[11] Li F, Su Z, Ye L and Meng G 2006 A correlation filtering-based matching pursuit (CF-MP) for damage identification using Lamb waves Smart Materials and Structures 15 6 1585-1594
[12] Liu L and Yuan F G 2008 Active damage localization for plate-like structures using wireless sensors and a distributed algorithm Smart Materials and Structures 17 1-12
[13] Zhang X, Qian T, Mei G, Kwan C, Zane R, Walsh C, Paing T and Popovic Z 2007 Active health monitoring of an aircraft wing with an embedded piezoelectric sensor/actuator network: II.Wireless approaches Smart Materials and Structures 16 1218–1225
[14] Michaels J E 2008 Effectiveness of in situ damage localization methods using sparse ultrasonic sensor arrays *Proceedings of the SPIE (Health Monitoring of Structural and Biological Systems)* 693510
[15] Michaels J E, Croxford A J and Wilcox P D 2008 Imaging Algorithms for Locating Damage via in situ Ultrasonic Sensors *IEEE Sensor Application Symposium* 63-67
[16] Grosse C U and Reinhardt H-W 1999 Schallemissionsquellen automatisch lokalisieren - Entwicklung eines Algorithmus Materialprüfung 41 9 342-347
[17] Moll J, Schulte R T, Hartmann B, Fritzen C-P and Nelles O 2010 Multi-site damage localization in anisotropic plate-like structures using an active guided wave structural health monitoring system Smart Materials and Structures (accepted for publication)
[18] Ng C T and Veidt M 2009 A Lamb-wave-based technique for damage detection in composite laminates Smart Materials and Structures 18 1-12
[19] Tua P S, Quek S T and Wang Q 2004 Detection of cracks in plates using piezo-actuated Lamb waves Smart Materials and Structures 13 4 643-660
[20] Moll J, Schulte R T and Fritzen C-P 2009 Damage Localization in Anisotropic Plates Using an Active Guided Wave Structural Health Monitoring System *7th International Workshop on Structural Health Monitoring (Stanford, USA)* 815-822